Vernier spectrum and isospin state control in carbon nanotube quantum dots

Jameson G. Berg,[1,*] Neda Lotfizadeh,[1,*] Dublin Nichols,[2] Mitchell J. Senger,[2] Wade DeGottardi,[3,†] Ethan D. Minot,[2,‡] and Vikram V. Deshpande[1,§]

[1]*Department of Physics and Astronomy, University of Utah, Salt Lake City, Utah 84112, USA*
[2]*Department of Physics, Oregon State University, Corvallis, Oregon 97331, USA*
[3]*Department of Physics, Texas Tech University, Lubbock, Texas 79409, USA*

(Received 18 April 2024; revised 7 August 2024; accepted 4 October 2024; published 1 November 2024)

Commensurability phenomena abound in nature and are typically associated with mismatched lengths, as can occur in quasiperiodic systems. However, not all commensuration effects are spatial in nature. In finite-sized Dirac systems, an intriguing example arises in tilted or warped Dirac cones wherein the degeneracy in the speed of right- and left-moving electrons within a given Dirac cone or valley is lifted. Bound states can be purely fast-moving or purely slow-moving, giving rise to incommensurate energy level spacings and a Vernier spectrum. In this work, we present evidence for this Vernier spectrum in Coulomb blockade measurements of ultraclean suspended carbon nanotube quantum dots. The addition-energy spectrum of the quantum dots reveals an energy-level structure that oscillates between aligned and misaligned energy levels. Our data suggest that the fast- and slow-moving bound states hybridize at certain gate voltages. Thus, gate-voltage tuning can select states with varying degrees of hybridization, suggesting numerous applications based on accessing this isospinlike degree of freedom.

DOI: 10.1103/PhysRevB.110.205401

I. INTRODUCTION

Commensuration [1] between scales is a ubiquitous phenomenon in physics, and it appears in areas as disparate as dislocations in epitaxial growth, moiré heterostructures, monolayer gas adsorbates, and superconducting vortex lattices. A daily-life example of commensuration is the Vernier scale used in the laboratory to make accurate length measurements. Commensuration phenomena are not strictly spatial. For instance, Vernier scales in frequency (so-called frequency combs) are used to perform Vernier spectroscopy [2]. This work explores commensuration effects between energy levels in finite-sized quantum systems, i.e., quantum dots (QDs).

Carbon nanotubes (CNTs) are clean one-dimensional systems that exhibit quantum coherent transport and are actively investigated for the development of quantum technologies [3,4]. Potential applications are supported by progress in the production, separation, and alignment of CNTs [5]. The possibility of commensuration effects in the energy spectra of single-walled CNT QDs was first predicted by Izumida *et al.* [6,7]. Such intrinsic electrical commensuration is connected to a host of other topics in contemporary CNT research [7–12].

Despite a significant body of experimental work on quantum bound states in CNTs, previous experiments have not observed a Vernier spectrum of energy levels. Single electron energy levels in CNT QDs are typically measured by electron transport experiments. The physics that is accessible in these experiments depends on (i) the length of the CNT, (ii) the environment surrounding the CNT, and (iii) the nature of the electrical contacts. Long CNTs can hold more electrons, which is needed to measure the energy-level spacing for hundreds of electrons. Ultraclean CNTs are required so electronic disorder does not disrupt patterns in the energy-level spacing. The electrical contacts must be either opaque or semitransparent so that single electron charging effects (Coulomb blockade) can facilitate the measurement of shell filling. Previous measurements of shell filling used short CNTs (a few hundred nanometers) [13,14]. Previous reports of long CNTs (>1 μm) in ultraclean environments (fully suspended) have used transparent contacts [15–17]. Our current work is unique because we study ultraclean suspended CNTs with semitransparent contacts and length >2 μm [see Fig. 1(a) for a device schematic].

In electron transport measurements of quantum dots, a gate voltage, V_g, is used to tune the number of electrons, N, that occupy the quantum dot. Transitions in occupation number (from N to $N+1$) are detected as a peak in zero-bias conductivity, as shown in Figs. 1(c) and 1(d) (Coulomb blockade peaks). If the electron energy levels of the QD have fourfold degeneracy, the Coulomb blockade peaks form groups of four [Fig. 1(c)]. If energy levels have twofold degeneracy, the Coulomb peaks form groups of two [Fig. 1(d)]. Further details about the energy-level structure can be extracted by measuring ΔV_g, the potential between consecutive Coulomb peaks. The potential ΔV_g is proportional to the energy required to add the Nth electron to the quantum dot [see the addition energy plots

*These authors contributed equally to this work.
†Contact author: wdegotta@ttu.edu
‡Contact author: ethan.minot@oregonstate.edu
§Contact author: vdesh@physics.utah.edu

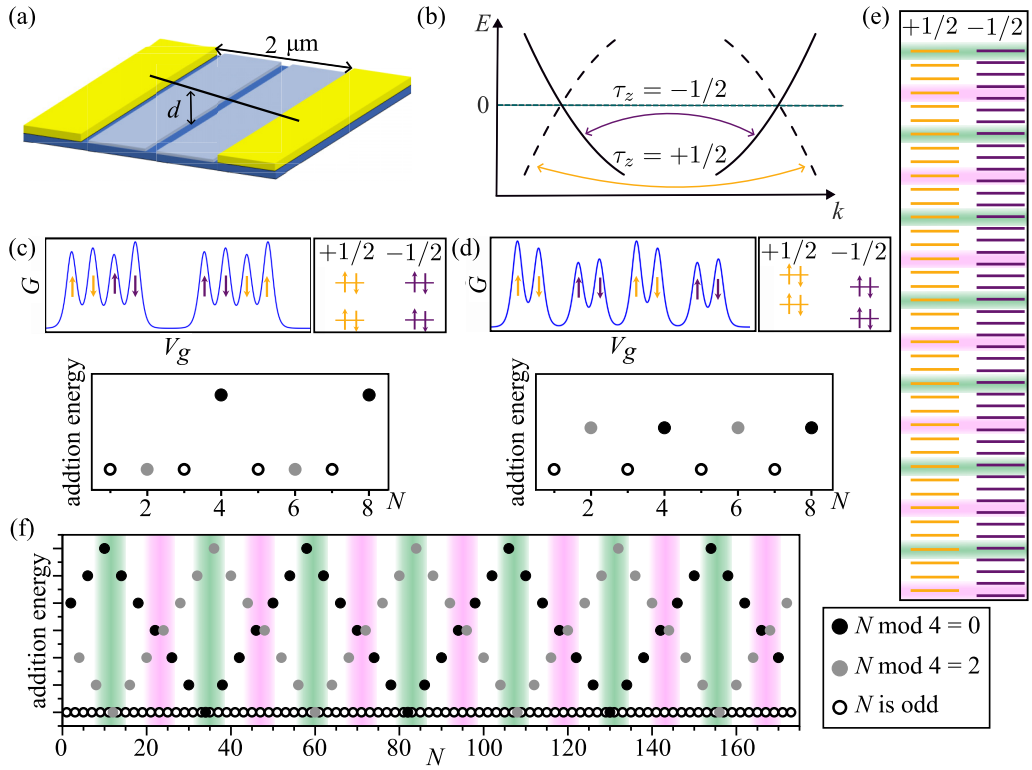

FIG. 1. (a) Schematic diagram of the suspended CNT quantum dot, with two gate electrodes under the CNT. Both gates are set to the same voltage, V_g. (b) Sketch showing the composition of a band-polarized state, which are formed from a superposition of a right- (left-) mover from one valley and a left- (right-) mover from the other valley. The band isospin is indicated by the quantum number $\tau_z = +1/2$ and $-1/2$. (c),(d) Sketch of conductance vs V_g (top panel) and addition energy vs electron number, N (bottom panel), for tubes in the quantum dot regime showing (c) four- and (d) two-electron periods, respectively. (e) For energies less than the charge neutrality, the energy level spacing associated with the $+1/2$ bands is greater than that in the $-1/2$ band. The mismatch in energy level spacing gives rise to the Vernier shell-filling spectrum. (f) The addition energy vs electron number, N, for a CNT with a Vernier energy spectrum exhibits characteristic peaks created by the transition between four- and two-period states. (Energies with four-electron periods noted in green and points of two-electron periods noted in pink.)

in Figs. 1(c) and 1(d)]. Previous literature on CNT QDs has sometimes reported fourfold shell filling [14,18] or twofold shell filling [13,19]. There have been no previous reports of a systematic oscillation between fourfold and twofold shell filling.

In our current work, we measure the addition energies of hundreds of electrons on long, ultraclean CNT QDs. We find oscillating patterns in the addition energies, matching the Vernier predictions of Izumida *et al.* We also find new features that were not previously predicted by theory. For example, some Vernier lobes are rounded, in contrast to the sharply peaked structures predicted by standard theory; moreover, adjacent lobes alternate in height. We extend existing theory to show that our experiment probes the degree of polarization/hybridization of the various quantum states probed in the system.

II. VERNIER SPECTRUM IN CARBON NANOTUBE QUANTUM DOTS

Figure 1(b) illustrates key features in the band structure of metallic CNTs, which are expected to produce a Vernier spectrum. There are two valleys centered at the K and K' points. Each valley hosts left-moving and right-moving electrons. The simplest model of CNT band structure predicts linear bands with symmetry between left-/right-moving states [19]. However, higher-order corrections such as trigonal warping [15–17] give rise to nonlinear bands and asymmetric velocities for left-/right-moving states. The velocity asymmetry was recently demonstrated in electron transport experiments on ultralong CNTs with transparent electrical contacts [15,16]. In the case of opaque or semitransparent contacts (as studied here), the CNT hosts electronic bound states with well-defined energy levels. Intervalley scattering at either end of the CNT couples a fast left-moving state in the K valley to a fast right-moving state of the K' valley [following the notation introduced by Izumida *et al.*, we use τ_z to denote this band degree of freedom; see the arrow labeled as $\tau_z = +1/2$ in Fig. 1(b)]. Similarly, a slow right-moving state of the K valley is coupled to a left-moving state of the K' valley [see the arrow labeled as $\tau_z = -1/2$ in Fig. 1(b)]. For energies below the charge-neutrality point (for holes), the level spacing between adjacent $\tau_z = +1/2$ states is slightly larger than for $\tau_z = -1/2$ states.

Figure 1(e) illustrates the energy level diagram resulting from a 14% mismatch in the level spacing of fast-moving versus slow-moving states. When the fast- and slow-moving states align in energy (highlighted in green), transport measurements would detect fourfold shell filling. When the fast- and slow-moving states are maximally misaligned (high-

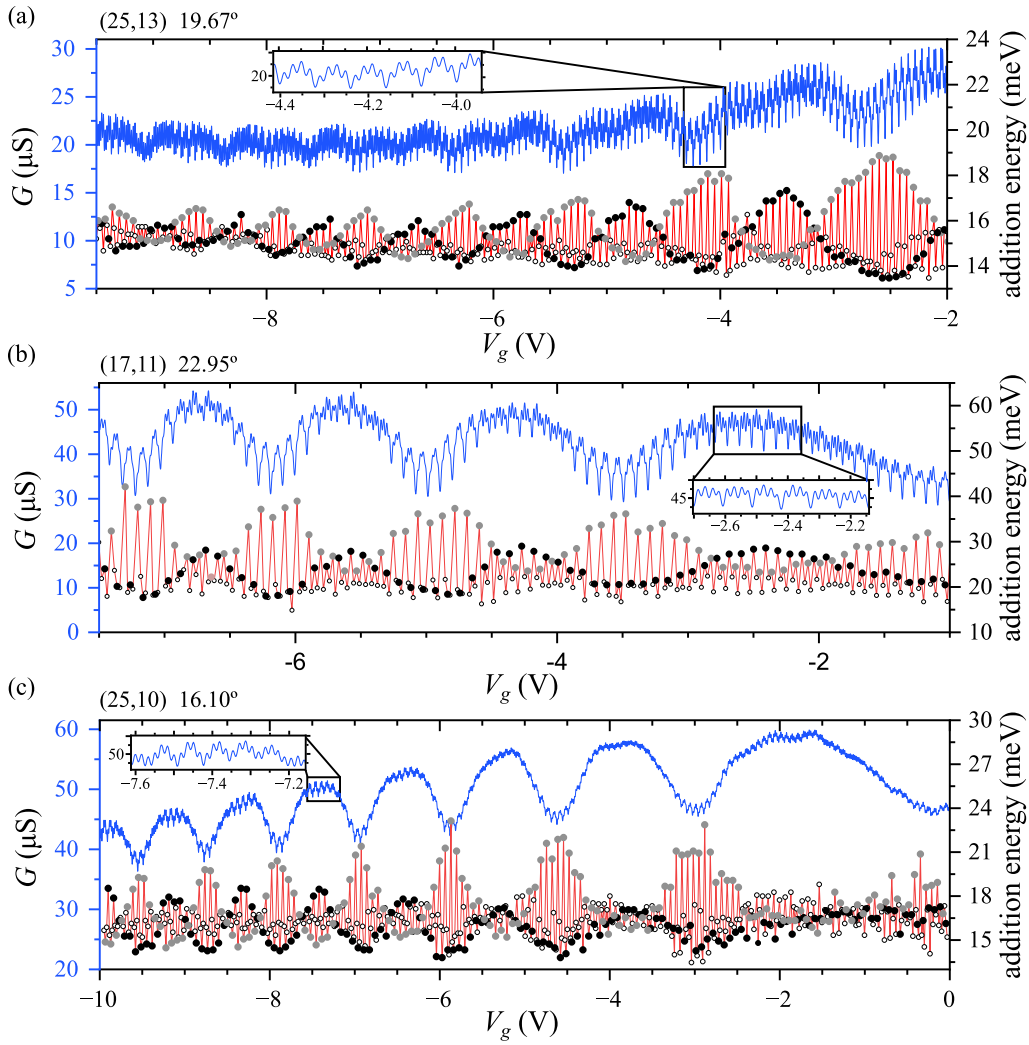

FIG. 2. (a)–(c) Measured conductance, G, vs V_g plotted in blue for Devices 1, 2, and 3 in the hole doped regime (negative V_g) at $T = 1.5$ K. Each device has clean shell filling peaks for over more than 400 electrons. The insets highlight representative clean shell filling peaks. Plotted in red is the corresponding addition energy for each electron added to the CNT, with N odd electrons marked with a white circle and N even electrons indicated by black (N mod 4 = 0) and gray (N mod 4 = 2) dots. All three devices show characteristic Vernier lobes in the addition energy graph. The Vernier lobes alternate in size in an even/odd pattern. Measured chiral indices and angles of each tube are noted in the top left corner of each plot.

lighted in pink), transport measurements would detect twofold shell filling. Figure 1(f) illustrates the addition energy spectra associated with Fig. 1(e). There is an oscillation between regions of fourfold shell (highlighted in green) and twofold shell filling (highlighted in pink). To visualize the structure of the oscillations, we color the addition of the Nth electron according to the value of N mod 4. The case of N odd is indicated by white dots, which form a flat baseline corresponding to the charging energy of the quantum dot. The case of N even is indicated by black (N mod 4 = 0) and gray (N mod 4 = 2) dots, which form interlacing tent-shaped structures, referred to here as Vernier lobes.

III. EXPERIMENTAL DETAILS AND RESULTS

Our measurements of suspended CNT quantum dots with length >2 μm were acquired at 1.5 K using a variable-temperature pumped helium cryostat. The CNTs were grown directly over the trenches via chemical vapor deposition using techniques detailed in previous works [20,21]. The chiral index of each CNT was determined using photocurrent spectroscopy [22]. Figure 2 shows three different tubes that all exhibit remarkably clean shell-filling Coulomb oscillations (see the insets of each tube) over a very large gate voltage range. The shell-filling oscillations are on top of long-period Sagnac oscillation (quantum interference effect) that results from the asymmetric velocities of charge carriers in the different bands [15,16]. Electron addition energies were extracted by measuring the gate voltage spacing between the maximum of each shell-filling peak. To ensure the true peak was extracted, a cubic spline interpolation was performed on the conductance data sets, the details of which are explained in S2 of the Supplemental Material [22]. Further, we used the coloring scheme for electron number modulo 4 as explained in Fig. 1(f) to reveal any substructure. The resulting color-coded addition energies and corresponding conductance plots are

shown in Fig. 2. Clear Vernier spectra are seen in all three tubes over a large range of gate voltage with interlacing black and gray dots. This pattern is present in every tube measured in the shell-filling regime (over 20 tubes), with the only exception being tubes where the level spacing is comparable to the thermal energy.

The Vernier shell-filling is characterized by various lobes. By comparing the theoretical shell-filling patterns in Fig. 1(f) with the data in Fig. 2, we see that the nodes of the Vernier lobes (crossing of black and gray dots) occur when the two bands are maximally separated in energy, which is associated with period 2 patterns of the addition energies [Fig. 1(d)]. The antinodes (maximum separation between black and gray) occur when the two bands have nearly degenerate energies, corresponding to a period 4 pattern of the addition energies [Fig. 1(c)]. A notable feature in our data is the charging energy of odd-numbered electrons (denoted by white dots). Unlike the standard theory [Fig. 1(f)], our experiments reveal variations in the floor associated with charging energy. In [22], we offer a model that accounts for some of the basic features of this effect. Another notable feature is the alternating size of the Vernier lobes, i.e., the peaks consisting of gray dots are a few meV higher than the peaks consisting of black dots. The most dramatic example is Device 3 [Fig. 2(c)], where the peak consisting of black dots does not exceed the minimum consisting of gray dots at $V_g = -3.7$ V. Such a pattern in lobe height is not predicted in theories of the Vernier spectrum in CNTs [6,7]. The rounding of the Vernier lobes seen in the data (Fig. 2) is suggestive of level repulsion, indicating that a perturbation is mixing the τ_z bands. It is unlikely that spin-orbit coupling is responsible for this effect since it does not play a significant role in tubes with Vernier shell-filling [6].

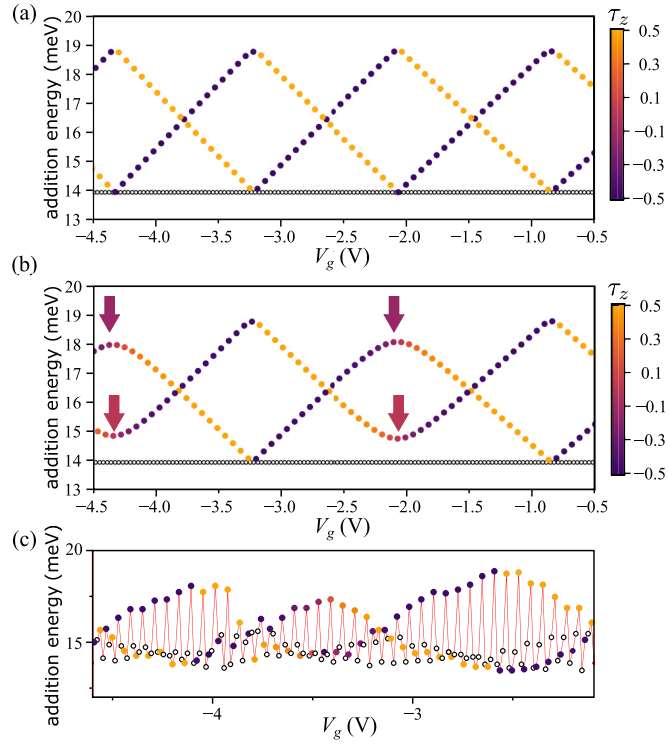

FIG. 3. (a) Calculated shell filling structure with no lead coupling ($V_0 = 0$) for a 2.5 μm tube with chiral indices (25,10). The electron number is with respect to half-filling. (b) Same as (a) with coupling turned on ($V_0 = 1$ meV and $a = 0.03\ L$). Color scheme shows the degree of hybridization of states between $\tau_z = +1/2$ and $-1/2$ and odd electrons denoted by white circles. In Vernier lobes with reduced peak heights, τ_z states become hybridized with arrows showing the points of maximal hybridization. (c) Section of addition energy from Fig. 2(a) with hybridization marked following the patterns present in the model.

IV. THEORETICAL MODEL

The conspicuous pattern of alternating heights of the black/gray Vernier lobes in Fig. 2 can be accounted for by considering the effect of contacts at either end of the CNT. As justified below, we consider a potential landscape that is sharply peaked near the ends of the tube,

$$V(x) = V_0 a[\delta(x) + \delta(x - L)], \tag{1}$$

where V_0 and a are phenomenological parameters with dimensions of energy and length, respectively. Potential (1) is a simplified description of a CNT interfaced to metal electrodes via semitransparent tunnel barriers. This potential acts as a perturbation of the low-energy electronic degrees of freedom of the tube, which are described by two gapless one-dimensional metallic bands [31]. Since the velocity asymmetry responsible for the Vernier spectrum depends on the chiral angle of the tube, our calculation takes as input a tube's chiral indices. For finite-sized tubes, the electron wave functions are standing waves. We take the basis state wave functions to be $\psi_\pm(x) = \cos(\pi n_\pm x/L)/\sqrt{2L}$, where L is the length of the nanotube and $n_\pm$ is the number of electrons in the $\tau_z = \pm 1/2$ bands, respectively [22]. For $V_0 = 0$, the shell-filling exhibits the sharply peaked Vernier lobes predicted by Refs. [6,7] and shown in Fig. 3(a). For finite V_0, level repulsion gives rise to rounding of the Vernier lobes and the alternating pattern associated with adjacent Vernier lobes. The latter arises due to the form of the potential (1) and the relative parities of the nearly degenerate states in different lobes. The parity of the state $\psi_\pm(x)$ is $P = (-1)^{n_\pm}$ so that within a given band, the parities of the states alternate with energy [6]. Given that the potential (1) is even about $x = L/2$, the matrix element between states of opposite parity vanishes, while it is nonzero between states of the same parity. In going from one Vernier lobe to the next, the number of states added with $\tau_z = +1/2$ and $-1/2$ differs by 1 and so the relative parity of the nearly degenerate states switches from one lobe to the next. As a result, if the matrix elements of $V(x)$ are zero between the nearly degenerate states in one lobe, then they are nonzero in the next. The effect of level repulsion alternates in strength, which is broadly consistent with the data. We note that this alternating pattern is inconsistent with an impurity potential somewhere in the middle of the tube, which would generally lead to an aperiodic pattern of envelope heights. Theoretical addition energies for a tube with parameters $V_0 = 1$ meV and $a = 0.03\ L$ are plotted in Fig. 3(b), where the extra even/odd Vernier lobe pattern is now present and resembles that of Fig. 2. Details of this calculation are provided in Ref. [22]. We also present a simulated shell-filling spectrum that accounts for Coulomb interactions. This simulation suggests that the

variation in the charging energy seen in Fig. 2 can also be attributed to potential (1) and thus corroborates its presence.

As a result of the coupling (1), the single-electron states are no longer pure eigenstates of τ_z but instead are hybridized. To quantify this, we have evaluated the expectation values $\langle\tau_z\rangle$ for the states in the simulated shell-filling spectra shown in Figs. 3(a) and 3(b). The hybridization pattern closely tracks the Vernier oscillations, with the nearly degenerate states [Fig. 3(b)] in every other Vernier lobe being maximally hybridized marked by arrows colored with the τ_z hybridization. Most other states are nearly pure band eigenstates with $\langle\tau_z\rangle \approx \pm 1/2$ [Fig. 3(a)]. Given the regularity of this pattern, we may estimate the degree of hybridization for actual data (Fig. 2) by comparing it with these theoretical predictions. The predicted degrees of hybridization are overlaid on the experimentally measured addition energies of Device 1 in Fig. 3(c). It is clear that the gate is able to tune the band quantum states from maximally polarized to hybridized. Such gate control over an isospin degree of freedom may be particularly useful in the study of valleytronics in the increasingly prevalent mixed-dimensional van der Waals heterostructures [32–36]. For example, in 1D-2D hybrid systems made from CNTs and graphene or transition-metal dichalcogenides (TMDs), it is predicted that valley coupling between the 1D and 2D systems with idealized band structures (i.e., without left/right asymmetry) leads to strong correlations and similar asymmetries and valley polarization/hybridization [37] as observed in our work.

V. CONCLUSION

In conclusion, a Vernier energy scale arises in finite-sized CNTs when the energy level structures of the isospin bands are incommensurate. In such a system, the addition energy spectrum for electron numbers $N \bmod 4 = 0$ and $N \bmod 4 = 2$ have a characteristic interwoven pattern that was previously predicted, but not previously observed. The quality of the transport data from our ultraclean suspended CNTs allowed us to observe this pattern over a large range of gate voltage and uncover new features of the system. The measured Vernier lobes have an alternating envelope height, which points to the coupling of the band isospin degree of freedom by an external potential associated with the ends of the nanotubes. We have used a phenomenological model to estimate the degree of isospin polarization for each of the energy states. This suggests that CNTs can serve as a gate-tunable platform to control the energy gap between isospin states, and furthermore, produce isospin states of any desired polarization. Taken together with the recent progress in the fabrication of hybrid mixed-dimensional systems using CNTs and graphene or TMDs, our work suggests the possibility of using CNTs as a source for quantum states whose isospin degree of freedom can be electrically tuned. This work has clear implications for valleytronic circuits.

ACKNOWLEDGMENTS

Work performed in Utah was supported in part by the National Science Foundation under Grant No. 2005182. Work in Oregon was supported by the National Science Foundation under Grant No. 2004968. Part of this research was conducted at the Northwest Nanotechnology Infrastructure, a National Nanotechnology Coordinated Infrastructure site at Oregon State University that is supported in part by the National Science Foundation (Grant No. NNCI-2025489) and Oregon State University. A portion of device fabrication was carried out in the University of California Santa Barbara (UCSB) nanofabrication facility.

The authors declare no competing interests.

[1] P. Bak, Commensurate phases, incommensurate phases and the devil's staircase, Rep. Prog. Phys. **45**, 587 (1982).

[2] N. Picqué and T. W. Hänsch, Frequency comb spectroscopy, Nat. Photon. **13**, 146 (2019).

[3] A. Baydin, F. Tay, J. Fan, M. Manjappa, W. Gao, and J. Kono, Carbon nanotube devices for quantum technology, Materials **15**, 1535 (2022).

[4] J. S. Chen, K. J. Trerayapiwat, L. Sun, M. D. Krzyaniak, M. R. Wasielewski, T. Rajh, S. Sharifzadeh, and X. Ma, Long-lived electronic spin qubits in single-walled carbon nanotubes, Nat. Commun. **14**, 1 (2023).

[5] A. D. Franklin, M. C. Hersam, and H. S. P. Wong, Carbon nanotube transistors: Making electronics from molecules, Science (1979) **378**, 726 (2022).

[6] W. Izumida, A. Vikström, and R. Saito, Asymmetric velocities of Dirac particles and Vernier spectrum in metallic single-wall carbon nanotubes, Phys. Rev. B **85**, 165430 (2012).

[7] W. Izumida, R. Okuyama, and R. Saito, Valley coupling in finite-length metallic single-wall carbon nanotubes, Phys. Rev. B **91**, 235442 (2015).

[8] W. Izumida, R. Okuyama, A. Yamakage, and R. Saito, Angular momentum and topology in semiconducting single-wall carbon nanotubes, Phys. Rev. B **93**, 195442 (2016).

[9] C. P. Moca, W. Izumida, B. Dóra, Ö. Legeza, J. K. Asbóth, and G. Zaránd, Topologically protected correlated end spin formation in carbon nanotubes, Phys. Rev. Lett. **125**, 056401 (2020).

[10] Y. Efroni, S. Ilani, and E. Berg, Topological transitions and fractional charges induced by strain and a magnetic field in carbon nanotubes, Phys. Rev. Lett. **119**, 147704 (2017).

[11] G. Buchs, M. Marganska, J. W. Gonzalez, K. Eimre, C. A. Pignedoli, D. Passerone, A. Ayuela, O. Groning, and D. Bercioux, Metallic carbon nanotube quantum dots with broken symmetries as a platform for tunable terahertz detection, Appl. Phys. Rev. **8**, 21406 (2021).

[12] M. C. Hels, T. S. Jespersen, J. Nygård, and K. Grove-Rasmussen, Coupling of shells in a carbon nanotube quantum dot, Phys. Rev. B **99**, 035422 (2019).

[13] D. H. Cobden and J. Nygård, Shell filling in closed single-wall carbon nanotube quantum dots, Phys. Rev. Lett. **89**, 046803 (2002).

[14] W. Liang, M. Bockrath, and H. Park, Shell filling and exchange coupling in metallic single-walled carbon nanotubes, Phys. Rev. Lett. **88**, 126801 (2002).

[15] A. Dirnaichner, M. del Valle, K. J. G. Götz, F. J. Schupp, N. Paradiso, M. Grifoni, C. Strunk, and A. K. Hüttel, Secondary

electron interference from trigonal warping in clean carbon nanotubes, Phys. Rev. Lett. **117**, 166804 (2016).
[16] N. Lotfizadeh, M. J. Senger, D. R. McCulley, E. D. Minot, and V. V. Deshpande, Quantum interferences in ultraclean carbon nanotubes, Phys. Rev. Lett. **126**, 216802 (2021).
[17] W. Yang, C. Urgell, S. L. De Bonis, M. Margańska, M. Grifoni, and A. Bachtold, Fabry-pérot oscillations in correlated carbon nanotubes, Phys. Rev. Lett. **125**, 187701 (2020).
[18] A. Makarovski, L. An, J. Liu, and G. Finkelstein, Persistent orbital degeneracy in carbon nanotubes, Phys. Rev. B **74**, 155431 (2006).
[19] E. A. Laird, F. Kuemmeth, G. A. Steele, K. Grove-Rasmussen, J. Nygård, K. Flensberg, and L. P. Kouwenhoven, Quantum transport in carbon nanotubes, Rev. Mod. Phys. **87**, 703 (2015).
[20] T. Sharf, J. W. Kevek, and E. D. Minot, Fabrication of low-noise carbon nanotube field-effect transistor biosensors, in *Proceedings of the IEEE Conference on Nanotechnology* (IEEE, Piscataway, NJ, 2011), Vol. 122.
[21] N. Lotfizadeh, D. R. McCulley, M. J. Senger, H. Fu, E. D. Minot, B. Skinner, and V. V. Deshpande, Band-gap-dependent electronic compressibility of carbon nanotubes in the wigner crystal regime, Phys. Rev. Lett. **123**, 197701 (2019).
[22] See Supplemental Material at http://link.aps.org/supplemental/10.1103/PhysRevB.110.205401 for details on the conductance and photocurrent spectroscopy measurements (S1), the interpolation scheme used to model the conductance (S2), and a description of the theoretical model used to calculate simulated shell-filling, which accounts for the putative potential at the ends of the tubes (S3), which includes Refs. [23–30].
[23] K. Liu *et al.*, An atlas of carbon nanotube optical transitions, Nat. Nanotechnol. **7**, 325 (2012).
[24] K. Liu *et al.*, Systematic determination of absolute absorption cross-section of individual carbon nanotubes, Proc. Natl. Acad. Sci. USA **111**, 7564 (2014).
[25] T. Deborde, L. Aspitarte, T. Sharf, J. W. Kevek, and E. D. Minot, Determining the chiral index of semiconducting carbon nanotubes using photoconductivity resonances, J. Phys. Chem. C **118**, 9946 (2014).
[26] M. J. Senger, D. R. McCulley, N. Lotfizadeh, V. V. Deshpande, and E. D. Minot, Universal interaction-driven gap in metallic carbon nanotubes, Phys. Rev. B **97**, 035445 (2018).
[27] T. DeBorde, J. W. Kevek, T. Sharf, J. L. Wardini, and E. D. Minot, A spectrally-tunable photocurrent microscope for characterizing nanoelectronic devices, in *Proceedings of the IEEE Conference on Nanotechnology* (IEEE, Piscataway, NJ, 2011), Vol. 382.
[28] L. Aspitarte, D. R. McCulley, and E. D. Minot, Photocurrent quantum yield in suspended carbon nanotube p-n junctions, Nano Lett. **16**, 5589 (2016).
[29] W. Degottardi, T. C. Wei, and S. Vishveshwara, Transverse-field-induced effects in carbon nanotubes, Phys. Rev. B **79**, 205421 (2009).
[30] R. Egger and A. O. Gogolin, Correlated transport and non-Fermi-liquid behavior in single-wall carbon nanotubes, Eur. Phys. J. B **3**, 281 (1998).
[31] C. Kane, L. Balents, and M. P. A. Fisher, Coulomb interactions and mesoscopic effects in carbon nanotubes, Phys. Rev. Lett. **79**, 5086 (1997).
[32] A. Cheng, T. Taniguchi, K. Watanabe, P. Kim, and J. D. Pillet, Guiding dirac fermions in graphene with a carbon nanotube, Phys. Rev. Lett. **123**, 216804 (2019).
[33] L. Anderson, A. Cheng, T. Taniguchi, K. Watanabe, and P. Kim, Coulomb drag between a carbon nanotube and monolayer graphene, Phys. Rev. Lett. **127**, 257701 (2021).
[34] S. Wang *et al.*, Gate-tunable plasmons in mixed-dimensional van der Waals heterostructures, Nat. Commun. **12**, 5039 (2021).
[35] D. Jariwala, T. J. Marks, and M. C. Hersam, Mixed-dimensional van der Waals heterostructures, Nat. Mater. **16**, 170 (2016).
[36] S. Annabi, E. Arrighi, A. Peugeot, H. Riechert, J. Griesmar, K. Watanabe, T. Taniguchi, L. Bretheau, and J.-D. Pillet, Ultraclean carbon nanotube-based Josephson junctions, arXiv:2405.19192.
[37] B. Flebus and A. H. MacDonald, Electronic structure of carbon nanotubes on graphene substrates, Phys. Rev. Res. **2**, 022041(R) (2020).